Characterization of insulin-degrading enzyme-mediated cleavage of Aβ in distinct aggregation states

Ellen Hubin [a,b,c], Federica Cioffi [a], Jef Rozenski [d], Nico A.J. van Nuland [b,c,*], Kerensa Broersen [a,**]

[a] Nanobiophysics Group, MIRA Institute for Biomedical Technology and Technical Medicine, Faculty of Science and Technology, Universiteit Twente, Enschede, The Netherlands
[b] Structural Biology Brussels, Vrije Universiteit Brussel, Pleinlaan 2, 1050 Brussels, Belgium
[c] Structural Biology Research Center, VIB, Pleinlaan 2, 1050 Brussels, Belgium
[d] Laboratory of Medicinal Chemistry, Rega Institute for Medical Research, KU Leuven, 3000 Leuven, Belgium

ARTICLE INFO

ABSTRACT

To enhance our understanding of the potential therapeutic utility of insulin-degrading enzyme (IDE) in Alzheimer's disease (AD), we studied in vitro IDE-mediated degradation of different amyloid-beta (Aβ) peptide aggregation states. Our findings show that IDE activity is driven by the dynamic equilibrium between Aβ monomers and higher ordered aggregates. We identify Met_{35}–Val_{36} as a novel IDE cleavage site in the Aβ sequence and show that Aβ fragments resulting from IDE cleavage form non-toxic amorphous aggregates. These findings need to be taken into account in therapeutic strategies designed to increase Aβ clearance in AD patients by modulating IDE activity.

© 2016 Elsevier B.V. All rights reserved.

1. Introduction

Alzheimer's disease (AD) patients generally show a decreased clearance of the amyloid-beta (Aβ) peptide compared to healthy control subjects [1]. The impairment of Aβ clearance, in some cases combined with an increased Aβ production, results in accumulation and assembly of Aβ into aggregated forms in the brain [2]. Therefore, lowering the Aβ burden by increasing Aβ clearance, e.g. by upregulating the activity of Aβ-degrading enzymes, provides a promising avenue for AD treatment [3,4].

Many proteases have been reported to cleave Aβ in vivo or in vitro, with insulin-degrading enzyme (IDE) and neprilysin (NEP) being the primary Aβ-cleaving enzymes [5–8]. Deficiencies of NEP and IDE resulted in the elevation of endogenous Aβ levels in the brain [9]. Also, a genetic association has been reported between single nucleotide polymorphisms in IDE and late-onset AD [10] and the deposition of Aβ was inversely correlated with NEP expression in TgCRND8 APP-transgenic mice [11]. IDE, a Zn^{2+}-metalloendopeptidase, has the ability to cleave Aβ intra- and extracellularly and may prove valuable as a target to upregulate Aβ clearance in impaired AD patients [12–14]. Administration of NEP or IDE reduces Aβ accumulation in the brain [8,15–17]. Intra-vitreal delivery of NEP reduced ocular levels of $Aβ_{1-40}$ and $Aβ_{1-42}$ in a dose-dependent manner [18]. Moreover, the membrane-bound form of NEP was observed to be active, apart from intracellular, towards extracellular residing Aβ as a result of facing of the active site towards the extracellular space [11] while it was demonstrated that IDE actively regulates extracellular levels of Aβ [19]. Therefore, drug compounds are under development that can modulate IDE activity to selectively enhance Aβ degradation, without affecting degradation of other IDE substrates such as insulin and amylin [20–22].

In view of the development of IDE-based AD therapies, more insight into the Aβ-degrading capacity of IDE is required. It has previously been reported that IDE is capable of degrading monomeric Aβ [23–26], but the effect of IDE on Aβ aggregates such as oligomers, suggested to be the primary toxic species in AD [27], and fibrils, is less well-documented in the literature. Moreover, the properties of IDE-induced fragments from Aβ are currently unknown. To extend our understanding of the potential therapeutic utility of IDE, we therefore monitored and characterized IDE-mediated cleavage of Aβ in vitro using biophysical techniques, at different time points during the Aβ aggregation process.

* Correspondence to: N. A.J. van Nuland, Structural Biology Brussels, Vrije Universiteit Brussel, Pleinlaan 2, 1050 Brussels, Belgium.
** Correspondence to: K. Broersen, Nanobiophysics Group (NBP), University of Twente, Zuidhorst ZH155, 7500 AE Enschede, The Netherlands.
E-mail addresses: nvnuland@vub.ac.be (N.A.J. van Nuland), k.broersen@utwente.nl (K. Broersen).

2. Material and methods

2.1. Aβ peptide solubilization

Aβ$_{1-40}$, Aβ$_{1-42}$, 15N-labelled Aβ peptides (rPeptide), Aβ$_{1-35}$, Aβ$_{36-40}$, and Aβ$_{36-42}$ (JPT Peptide Technologies GmbH) were dissolved according to the standard procedure developed and validated in our laboratory [28]. In short, Aβ peptides were dissolved in hexafluoroisopropanol (HFIP). HFIP was evaporated using nitrogen gas and the peptide film was redissolved using dimethyl sulfoxide (DMSO). The peptide was separated from DMSO by elution from a HiTrap™ desalting column (GE Healthcare) into the appropriate filtered buffer (Thioflavin T (ThT) fluorescence measurements: PBS pH 7.4, electrospray ionization mass spectrometry (ESI-MS): 100 mM NH$_4$HCO$_3$ pH 7.4, nuclear magnetic resonance (NMR): 50 mM phosphate buffer pH 6.8 containing 50 mM NaCl). The resulting samples were kept on ice until experiments started with a maximum lag time of 30 min. Peptide concentration was determined using the Coomassie (Bradford) Protein Assay kit and diluted to the required final concentration. Aggregation of Aβ peptides occurred at 37 °C under quiescent conditions.

2.2. Proteolytic degradation of Aβ by IDE and NEP

Recombinant human IDE (cat. no. 2496-ZN-010) and NEP (cat. no. 1182-ZNC-010) were commercially obtained from R&D Systems and tested for purity using SDS-PAGE, both under reducing and under non-reducing conditions and visualized by silver stain (Fig. S1). IDE was added to Aβ samples at a final concentration of 36 nM at the beginning of the aggregation process, after 3 h, and after 21 h and later. Under these conditions but in the absence of IDE, samples comprise mainly Aβ monomers (0 h), oligomers (3 h), and (proto)fibrils (21 h and later), as demonstrated by Broersen et al. [28]. IDE-mediated cleavage of Aβ was monitored using ThT fluorescence, ESI-MS, and solution NMR. For the latter, NEP was added to the NMR sample at a concentration of 36 nM.

2.3. ThT fluorescence to monitor peptide aggregation/cleavage

The fibril formation kinetics of 10 μM peptide sample preparations were monitored in situ by measuring fluorescence of ThT (12 μM) at 37 °C in a Greiner 96-well plate using a FLUOstar OPTIMA fluorescence plate reader (BMG LABTECH GmbH, Germany) at an excitation wavelength of 440 nm (9 nm bandwidth) and an emission wavelength of 480 nm (20 nm bandwidth). Fluorescence readings were recorded in triplicates. Recorded values were averaged and background measurements (buffer containing ThT, with or without IDE) were subtracted.

2.4. Identification of generated Aβ fragments upon IDE cleavage using ESI-MS

ESI-MS was used to identify Aβ fragments generated by IDE [29]. Positive-ion mass spectra were recorded on an orthogonal acceleration quadrupole time-of-flight mass spectrometer (Synapt G2 HDMS, Waters, Milford, MA) equipped with a standard electrospray probe (Z-spray) and controlled by a datasystem running MassLynx 4.1 (Micromass, Manchester, UK), which was also used for spectra analysis and peptide fragment identification. Samples were diluted 1:10 in acetonitrile:water (1:1) prior to immediate infusion using a syringe pump with a flow rate of 5 μl/min. Cone voltage was set to 30 V, capillary voltage was 3 kV. Scan time was set to 4.9 s with an inter-scan time of 0.1 s. At least ten spectra were acquired for two independent experiments and averaged for each condition.

2.5. Solution NMR spectroscopy to monitor Aβ aggregation/cleavage

Prior to incubation, 50 μl D$_2$O was added to 15N-labelled Aβ (45 μM final concentration) to reach a final volume of 550 μl. The 2D 1H–15N heteronuclear single quantum correlation spectroscopy (HSQC) experiments were conducted at 37 °C with a Varian NMR Direct-Drive System 800 MHz spectrometer equipped with a salt tolerance triple-resonance PFG-Z cold probe. Data were processed using NMRPipe [30] and analysed using CCpNMR [31]. Water was suppressed by 3-9-19 watergate pulses, while coherence selection was achieved by echo–antiecho pulsed-field gradients. The HSQC spectra were acquired with spectral widths of 14.2 ppm and 24 ppm in 1H and 15N dimensions, respectively, and 2048 and 64 complex points in the direct and indirect dimensions, respectively.

2.6. In silico prediction of peptide aggregation

The statistical mechanics-based algorithm TANGO predicts protein aggregation [32]. For each residue in a protein, TANGO computes the percent occupancy of the β-aggregation conformation. Proteins possessing segments of at least five consecutive residues populating the β-aggregated conformation (each with a score higher than 5%) are considered to have the tendency to aggregate. TANGO calculations were performed via http://tango.switchlab.org/ for the peptides under study at a pH 7.4, 298.15 K, 0.02 M ionic strength, and without N- or C-terminal protection.

2.7. Transmission electron microscopy of peptide aggregates

After 24 h of incubation at a concentration of 10 μM, peptides (5 μl) were adsorbed to carbon-coated Formvar 400-mesh copper grids (Agar Scientific) for 1 min. The grids were washed, blotted, and stained with 1% (w/v) uranyl acetate. Samples were studied using transmission electron microscopy (TEM) with a JEM-1400 microscope (JEOL Ltd., Tokyo, Japan) at 80 kV. Reported TEM images are representative of three independent experiments.
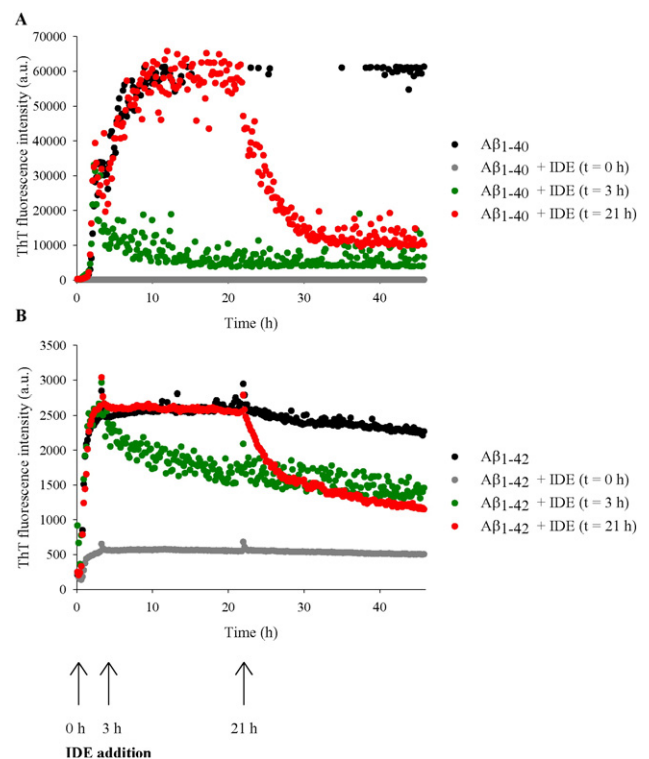

Fig. 1. Aβ aggregation state determines susceptibility for IDE-mediated degradation. Aggregation of 10 μM (A) Aβ$_{1-40}$ and (B) Aβ$_{1-42}$ was monitored by ThT fluorescence. IDE (36 nM) was added at the beginning of the Aβ aggregation process (sample comprising mainly Aβ monomers), after 3 h (enriched in oligomers), and after 21 h (enriched in (proto)fibrils).

2.8. Dotblot with toxic oligomer-specific A11 antibody

At specific aggregation time points, 5 µl peptide was spotted onto a nitrocellulose membrane. The membranes were blocked in phosphate buffered saline containing 0.2% Tween-20 (1 h, 25 °C), and incubated (overnight, 4 °C) with primary A11 antibody (Invitrogen), diluted 1:4000 in 100 mM Hepes, pH 7.0 [33]. After incubation (0.5 h, 25 °C) with a secondary anti-rabbit-HRP-tagged antibody (Promega), diluted 1:5000 in phosphate buffered saline containing 0.05% Tween-20, the membranes were visualized using the Immobilon™ Western chemiluminescent HRP substrate system. Experiments were carried out in duplicates.

2.9. Cytotoxicity of Aβ fragments

SH-SY5Y cells were grown in DMEM/F12 supplemented with 10% FBS, 1% penicillin/streptomycin and 1% nonessential amino acids (Gibco). Cells were seeded in a 96-well plate at 25,000 cells/well and maintained in phenol-red free DMEM/F12 (L-Glutamine, 15 mM HEPES) supplemented with and 1% penicillin/streptomycin and placed incubated at 5% CO_2. Samples containing $A\beta_{1-40}$, $A\beta_{1-42}$, $A\beta_{1-35}$, $A\beta_{36-40}$, and $A\beta_{36-42}$ were pre-incubated at room temperature for 2 h, diluted in DMEM/F12 and added to the cells at a final concentration of 25 µM. An amount of 2 µM staurosporine (Sigma-Aldrich) was used as positive control. The plates were incubated at 37 °C for 48 h, followed by addition of CellTiter-Blue® Reagent (20 µl/well) and incubation for 4 h. The fluorescence (excitation: 560 nm and emission 590 nm) was measured using a TECAN Infinite 200 PRO fluorescence platereader. The medium background values were subtracted from the values obtained in experimental wells. Statistical significance of the results was established by P-values using two-tailed t-tests (GraphPad Software). Values represent results of three independent replicates. Statistical significance levels were $*P < 0.05$, $**P < 0.01$ and $***P < 0.001$ compared with the control group cells.

3. Results and discussion

3.1. Aβ aggregation state determines susceptibility to degradation by IDE

The effect of IDE on various Aβ aggregated species was initially assessed by monitoring changes in ThT fluorescence, as this is a commonly used reporter dye for fibril formation [34]. In the absence of IDE, $A\beta_{1-40}$ aggregation at 37 °C was marked by a strong increase in ThT fluorescence, indicative of fibril formation. In contrast, addition of IDE to monomeric $A\beta_{1-40}$ prevented ThT-positive fibril formation within the time frame of the measurements, as the ThT background signal did not increase. This shows that IDE is capable of degrading $A\beta_{1-40}$ monomers into fragments that do not form ThT-positive aggregates upon prolonged incubation (Fig. 1A), and
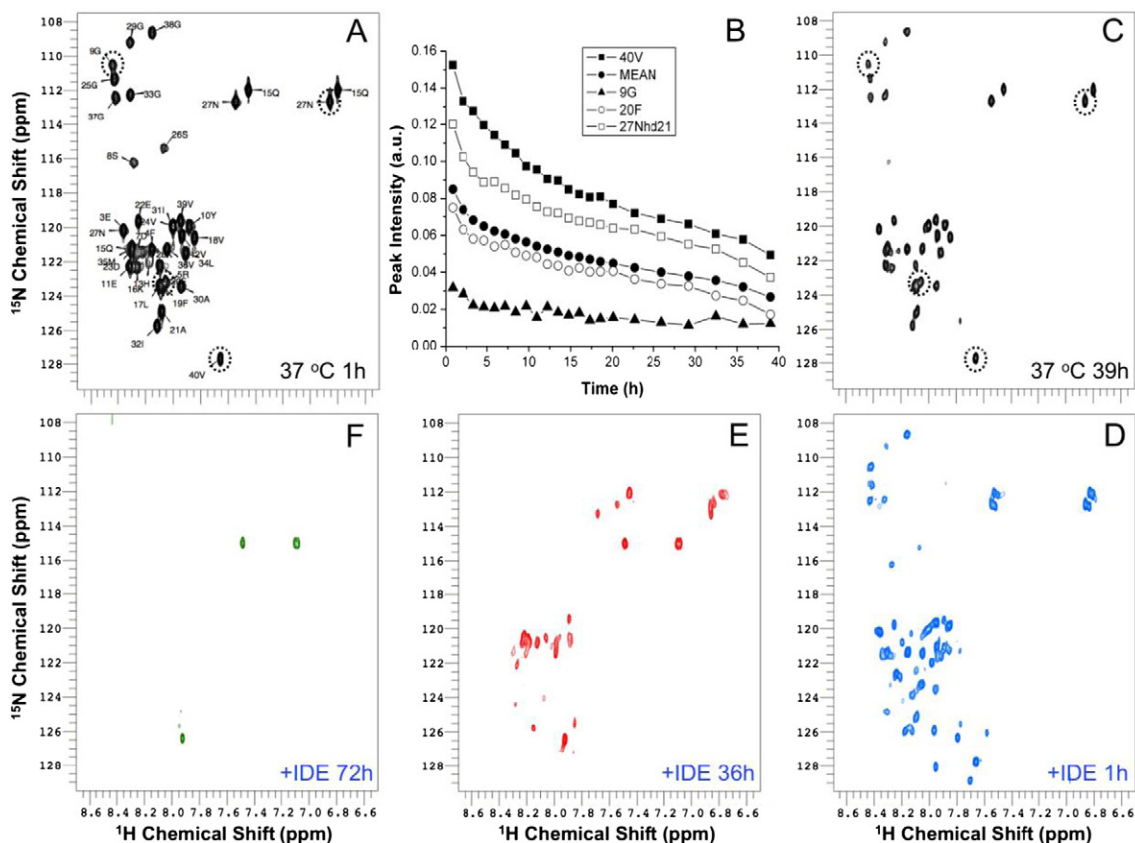

Fig. 2. Aggregation and cleavage of $A\beta_{1-40}$ monitored by solution NMR spectroscopy. (A) 1H–15N HSQC spectrum of $A\beta_{1-40}$ (45 µM) at 37 °C recorded within 1 h after initiating the aggregation process. Peak assignments of the 1H–15N HSQC spectrum of $A\beta_{1-40}$ were transferred from previous studies [41,50,51]. (B) Decrease in 1H–15N HSQC signal intensity upon aggregation of $A\beta_{1-40}$ for selected signals of 9G, 20E, 27NHd21 and 40V (encircled in A and C). For comparison, the decrease in the average of all signals (MEAN) is also shown. (C) 1H–15N HSQC spectrum of $A\beta_{1-40}$ at 37 °C recorded within 39 h after initiating the aggregation process. (D–F) 1H–15N HSQC spectra of $A\beta_{1-40}$ recorded within 1 h (D), 36 h (E) and 72 h (F) after addition of IDE (36 nM) to aggregated $A\beta_{1-40}$ (shown in C). Spectra at early time points (D) show new peaks, and re-appearance, shifting and splitting of original peaks. However, the signal intensity decays in time (E and F), indicating that the generated fragments also aggregate, or stick to larger aggregates still present in the sample. All spectra are plotted at the same contour level.

is in agreement with previous studies [23–26]. In contrast, IDE addition at later Aβ aggregation time points, enriched in oligomers (3 h) or (proto)fibrils (21 h) [28], induced a partial decrease in ThT fluorescence suggesting that ThT-positive aggregates were retained in the solution in the presence of the enzyme. The cleavage of Aβ$_{1-42}$ by IDE showed many similarities with the observations for Aβ$_{1-40}$. IDE-mediated Aβ$_{1-42}$ cleavage was characterized by a strong inhibition of Aβ$_{1-42}$ fibril formation when IDE was added at the beginning of the aggregation process. However, a small increase in ThT fluorescence was apparent, reflecting the higher aggregation propensity of Aβ$_{1-42}$ compared to Aβ$_{1-40}$. The decrease in ThT fluorescence when IDE was added at later aggregation time points was also detected

for Aβ$_{1-42}$, but less pronounced compared to Aβ$_{1-40}$ (Fig. 1B). This partial decrease suggests (i) degradation of ThT-positive Aβ aggregates by IDE, or (ii) degradation of monomers in solution that is in dynamic equilibrium with ThT-positive aggregates, causing dissociation of ThT-positive aggregates to restore this equilibrium. Recent structural reports of IDE point in the direction of the latter hypothesis, as the crystal structure of IDE resembles a clamshell with a large internal chamber formed from two bowl-shaped halves connected by a flexible linker. IDE engulfs and degrades its substrates within this catalytic chamber whose size is limited to accommodate only relatively small peptides, *i.e.* consisting of maximally 70 amino acids [35–37]. The ThT fluorescence data reported here would
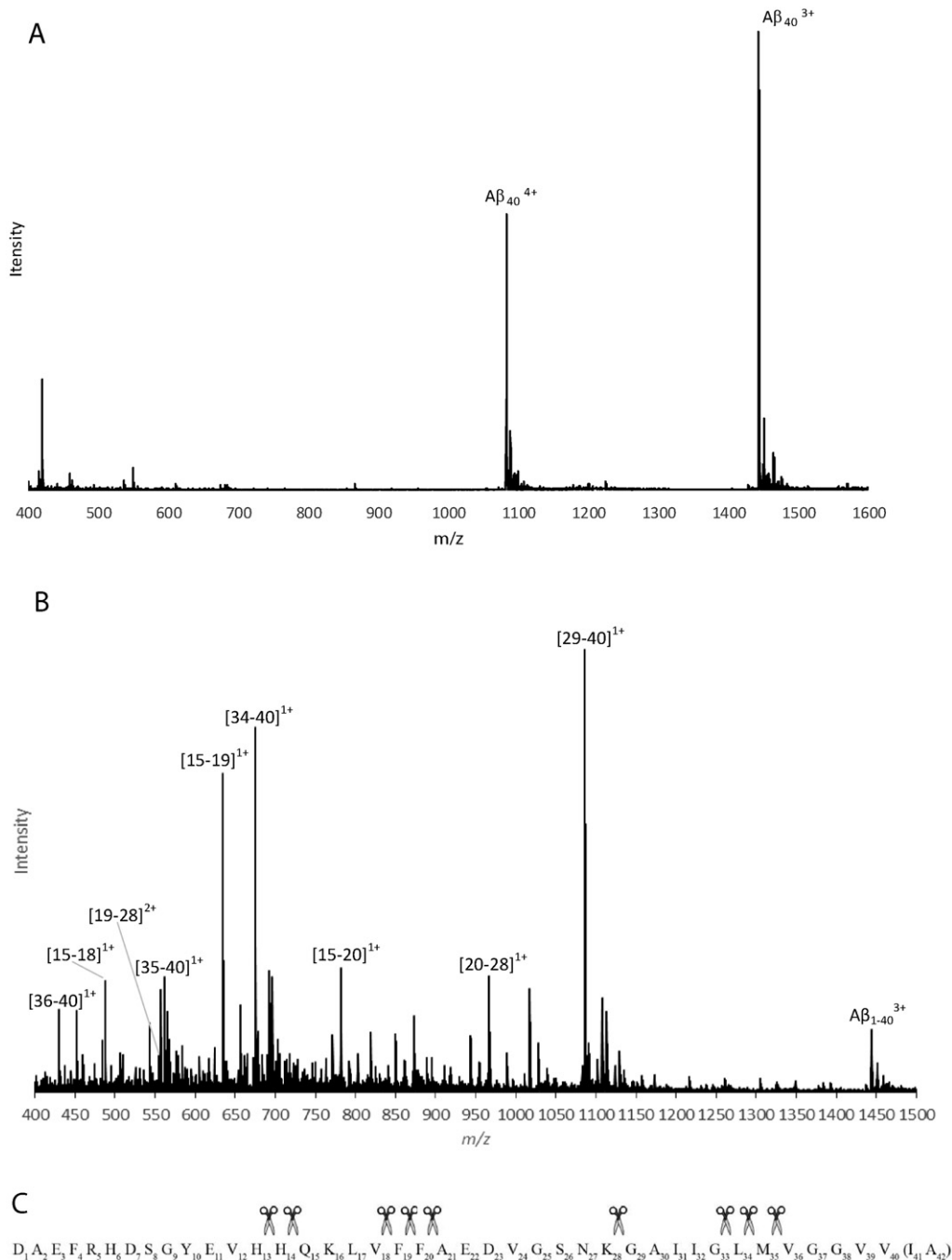

Fig. 3. IDE-mediated cleavage of monomeric Aβ results in multiple fragments. Assignment of ion peaks detected by ESI-MS associated with monomeric Aβ$_{1-40}$ (10 μM) in (A) the absence and (B) presence of 36 nM IDE, after 15 min of incubation at 37 °C. (C) Overview of the detected Aβ$_{1-40}$ and Aβ$_{1-42}$ sites susceptible to IDE proteolysis.

therefore be in agreement with the hypothesis that IDE exclusively degrades monomeric Aβ, because oligomeric and fibrillar forms of Aβ are too large to completely fit into this previously identified catalytic chamber [35–38]. Biological significance can be addressed to this observation as the presence of IDE appears to induce a displacement in monomer-aggregate equilibrium, potentially steering the Aβ assembly pathway away from toxic oligomer formation.

To further characterize IDE-mediated Aβ cleavage, degradation of 15N-labelled Aβ by IDE was monitored using $1H-^{15}N$ heteronuclear NMR spectroscopy. Solution NMR has the advantage that only small species, i.e. Aβ monomers and early oligomers, are detectable as the resonances broaden and signal intensities decrease due to long rotational correlation times when aggregation ensues [39]. Accordingly, 15N-labelled $Aβ_{1-40}$ aggregation was accompanied by a systematic slow decrease of all peak intensities in time (Fig. 2A–B). However, after 39 h of incubation of $Aβ_{1-40}$ at 37 °C, some residual signal intensity was still present (Fig. 2C). This is in agreement with previous studies showing a decrease in intensity for the backbone amides until a dynamic equilibrium is established between monomers and higher ordered aggregates [40,41] while the effect of enzymatic activity towards specific species within this equilibrium had not been observed before. As $Aβ_{1-42}$ aggregation is much faster, we first recorded a reference HSQC spectrum at 25 °C (Fig. S2A) before increasing the temperature to 37 °C. Indeed, all peaks disappeared within 4 h at 37 °C (Fig. S2B–C). Addition of IDE to the aggregated Aβ samples resulted in reappearance of the peak intensities and changes in chemical shifts of some peaks (results for $Aβ_{1-40}$ in Fig. 2 and for $Aβ_{1-42}$ in Fig. S2). Several new peaks emerged, and other peaks were shifted or split in comparison with the original spectrum. These findings reflect changes in the local environment of certain amino acids, caused by the formation of different Aβ fragments upon IDE cleavage. However, in light of the findings derived from the structural IDE studies mentioned above, the species that were cleaved by IDE are most likely Aβ monomers in dynamic equilibrium with NMR-invisible aggregates, and not the aggregates themselves. Previous studies using solution NMR demonstrated that Aβ monomers are constantly binding to and being released from oligomers [40] and protofibrils [41],

making this hypothesis feasible although it requires validation by future experiments.

Although hydrogen-deuterium exchange MS showed that Aβ molecules making up fibrils are also continuously recycled [42], no peaks reappeared in HSQC spectra after IDE addition to mature fibrils. However, a mixture of Aβ-degrading enzymes is present in vivo with different Aβ-degrading capacities. It is thus possible that Aβ aggregates that were not or only partially degraded by IDE are sensitive to yet other known enzymes with Aβ-degrading activity. We tested this hypothesis by adding a second Aβ-degrading enzyme, i.e. NEP, to an aggregated $Aβ_{1-42}$ sample that had first been subjected to IDE. We found that NEP addition resulted in the appearance of new peaks and shifting/splitting of other peaks (Fig. S2G–H). This observation indicates that combination therapy, based on the distinct degrading capacities of different proteases, might have therapeutic utility.

3.2. Aβ degradation by IDE in vitro results in multiple fragments reported in vivo

To investigate which fragments are formed upon IDE-mediated cleavage of Aβ, the cleavage fingerprints of $Aβ_{1-40}$ and $Aβ_{1-42}$ by IDE were determined using ESI-MS. Our results show that monomeric $Aβ_{1-40}$ and $Aβ_{1-42}$ are cleaved at multiple and similar sites (results for $Aβ_{1-40}$ in Fig. 3 and for $Aβ_{1-42}$ in Fig. S3), which is in agreement with previous in vitro studies [23–26,43]. Several Aβ fragments reported here have also been detected in the cerebrospinal fluid and plasma of AD patients [44–47]. The data reported here confirm the recently discovered cleavage sites $Gly_{33}-Leu_{34}$ and $Leu_{34}-Met_{35}$ [43] and identify $Met_{35}-Val_{36}$ as a novel cleavage site, resulting in the release of fragments $Aβ_{1-35}$ and $Aβ_{36-40}/Aβ_{36-42}$. For several cleavage sites however, only the corresponding N- or C-terminal fragment was detected in the mass spectrum, as not all fragments are ionized efficiently, were aggregated or degraded prior to entry in the mass spectrometer. As the N-terminal fragment of novel cleavage site $Met_{35}-Val_{36}$ could not be observed, the observation of this cleavage site was further confirmed using additional MS/MS analysis by comparing mass spectra of the IDE-induced fragments $Aβ_{36-40}/Aβ_{36-42}$
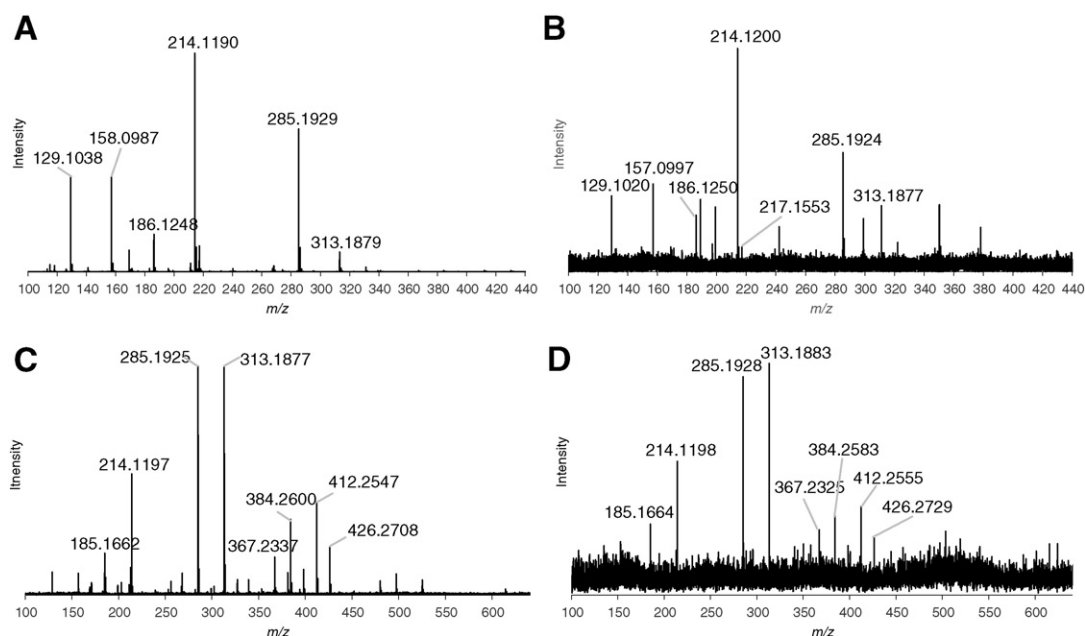

Fig. 4. Confirmation of Aβ fragments 36–40/36–42. MS/MS of (A) $Aβ_{36-40}$ fragment obtained upon IDE-mediated cleavage of $Aβ_{1-40}$, (B) synthetically derived $Aβ_{36-40}$ fragment, (C) $Aβ_{36-42}$ fragment obtained upon IDE-mediated cleavage of $Aβ_{1-42}$, and (D) synthetically derived $Aβ_{36-42}$ fragment.

with that of synthetically derived peptide fragments (Fig. 4). Moreover, fragments $A\beta_{14-28}$, $A\beta_{15-28}$, and $A\beta_{20-28}$ were detected, indicating that one Aβ peptide can be cleaved by IDE at least twice, *e.g.* at His$_{13}$–His$_{14}$ and consecutively at Lys$_{28}$–Gly$_{29}$ (Fig. 3 — Fig. S3). As one of the roles of IDE is to completely inactivate hormones such as insulin [48], this could explain why it cleaves its substrates at multiple sites, to ensure elimination of any residual activity.

IDE addition to aggregated Aβ resulted in similar fragments compared to addition of IDE to monomeric Aβ, but there was a considerable amount of non-degraded Aβ peptide left in the sample (denoted by asterisks in Fig. 5). This can be seen by the higher intensities of the ion peaks corresponding to full-length Aβ (Aβ^{3+} at *m/z* 1443.0, Aβ^{4+} at *m/z* 1083.3) compared to the most intense generated fragment $A\beta_{20-40}$ (Aβ^{2+}_{20-40} at *m/z* 1017.5) in Fig. 5B. This, together with the lack of reappearance of 1H–15N peak intensities after addition of IDE to mature fibrils, implies that increasing Aβ fibril maturity correlates with a decreased propensity to IDE-mediated cleavage.

3.3. Fragments generated by IDE-mediated Aβ degradation are aggregation-prone but not toxic

The properties of the obtained fragments upon IDE cleavage of Aβ have not yet been fully explored. This is however crucial in light of the development of IDE-based therapeutic AD strategies, as one must assure that fragments generated upon increased proteolytic activity are not aggregation-prone themselves.

ThT fluorescence data indicate that no ThT-positive aggregates were formed from the Aβ fragments obtained upon IDE cleavage of monomeric Aβ (Fig. 1). However, ThT fluorescence may not provide the most sensitive read-out to detect small quantities of aggregation, possibly formed only by a specific subset of fragments. Alternatively, resulting aggregated fragments might have less or no affinity for ThT. Previous studies indicate that the ThT dye binds to surface side-chain grooves running parallel to the axis of the β-sheets, that are characteristic of amyloid fibrils [49]. A model has been proposed in which five aligned aromatic and/or hydrophobic residues are critical for ThT binding [34]. It is thus possible that the Aβ fragments studied here lack the minimal ThT binding site.

Insight into the behaviour of these fragments was therefore obtained by more sensitive techniques. First, the disappearance of the 1H–15N HSQC signal corresponding to $A\beta_{1-40}$ in Fig. 2C–E, as seen by comparing the peak intensities after different time points of incubation with IDE, suggests that the generated Aβ fragments aggregate themselves or stick to larger remaining aggregates in the sample. Accordingly, ESI-MS revealed the presence of several fragments in the
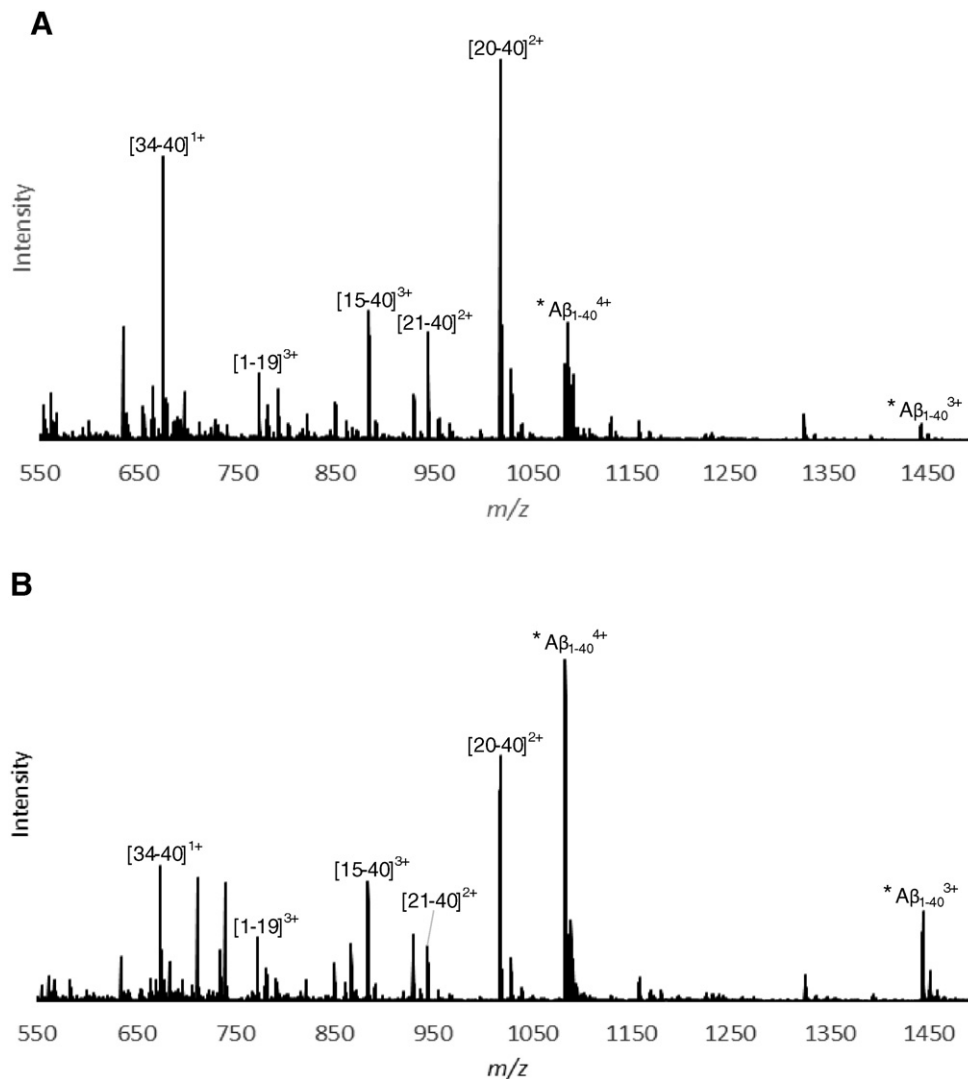

Fig. 5. Longer incubation times of Aβ prior to IDE addition result in a decrease in susceptibility of Aβ for IDE-mediated cleavage. Assignment of $A\beta_{1-40}$ fragments detected by ESI-MS. IDE (36 nM) was added to an $A\beta_{1-40}$ (10 μM) buffered solution at (A) t = 0 h and (B) t = 24 h of the aggregation process, and incubated for 1 h at 37 °C. Samples were centrifuged for 15 min at 13,200 rpm prior to ESI-MS analysis and the data depicted here correspond to the soluble fractions. Non-degraded Aβ peptide remaining in the sample is indicated by an asterisk.

pellet fractions, obtained after prolonged incubation of Aβ with IDE, demonstrating their aggregation propensity (Fig. 6).

Next, the properties of the newly identified Aβ fragments (Aβ$_{1-35}$ and Aβ$_{36-40}$/Aβ$_{36-42}$) were investigated in more detail. TANGO, a statistical mechanics-based algorithm, predicts protein aggregation for Aβ$_{1-35}$ and to a lesser extent for Aβ$_{36-42}$ (Fig. S4). Both peptides contain one or both of the aggregation nucleating regions previously reported for Aβ$_{1-42}$, *i.e.* the regions encompassing residues 17–21 and 30–42. In contrast, no aggregation propensity was predicted for Aβ$_{36-40}$. To assess the validity of the *in silico* predictions, the aggregation behaviour of the peptides was monitored using ThT fluorescence at 37 °C. Aβ$_{1-35}$ displayed a ThT sigmoidal curve, characteristic of Aβ aggregation, but with an extended lag phase of 10 h and a lower final ThT fluorescence intensity compared to Aβ$_{1-42}$ (Fig. 7A–B). In contrast, Aβ$_{36-40}$ and Aβ$_{36-42}$ did not stain ThT-positive, even after 72 h of incubation (Fig. 7B). However, TEM imaging revealed amorphous aggregates for all fragments, in contrast to the dense network of amyloid fibrils formed by Aβ$_{1-42}$ (Fig. 7C). As these amorphous aggregates show less or no sensitivity to ThT staining, they might lack the channels/sites necessary for ThT binding [34]. As a final assessment of the properties of these peptide fragments, a dot blot analysis was carried out with the oligomer-specific A11 antibody. Aβ oligomers have previously been reported to be responsible for the neurotoxicity and cognitive defects in AD patients [27]. A high A11 response was detected for Aβ$_{1-42}$ (included as a reference) after 1.5 h of incubation (Fig. 7D), which has been demonstrated to correspond to a toxic Aβ oligomer-enriched fraction [28]. Aggregation into higher aggregates coincided with a decrease in A11 intensity. In contrast, A11 reactivity was not detected in the case of any of the Aβ fragments. Cell viability assays further showed that these aggregated forms of Aβ fragments were not toxic to neuroblastoma cells (Fig. 7E). In summary, although the fragments under study do not form A11-positive oligomers, they do result in non-toxic amorphous aggregates with no or less ThT staining (compared to Aβ$_{1-42}$). The aggregation-prone character of these Aβ fragments should be considered when developing modulators to enhance the proteolytic activity of IDE while their non-toxic character further strengthens the therapeutic potential use of IDE and NEP proteolytic activities.

4. Conclusion

In conclusion, we show that Aβ monomers, either alone in solution or in dynamic equilibrium with higher aggregates, are cleaved at multiple sites by IDE. We report a new Aβ cleavage site, *i.e.* Met$_{35}$–Val$_{36}$, and show that the resulting Aβ fragments form non-toxic amorphous aggregates that are not or less sensitive for ThT staining. The generation of Aβ fragments that are aggregation-prone must be considered when developing IDE-based strategies targeting AD. Moreover, combining proteases capable of degrading different Aβ aggregation species at distinct cellular locations, such as IDE, NEP, and matrix metalloproteinase-9, might hold therapeutic potential for AD treatment.
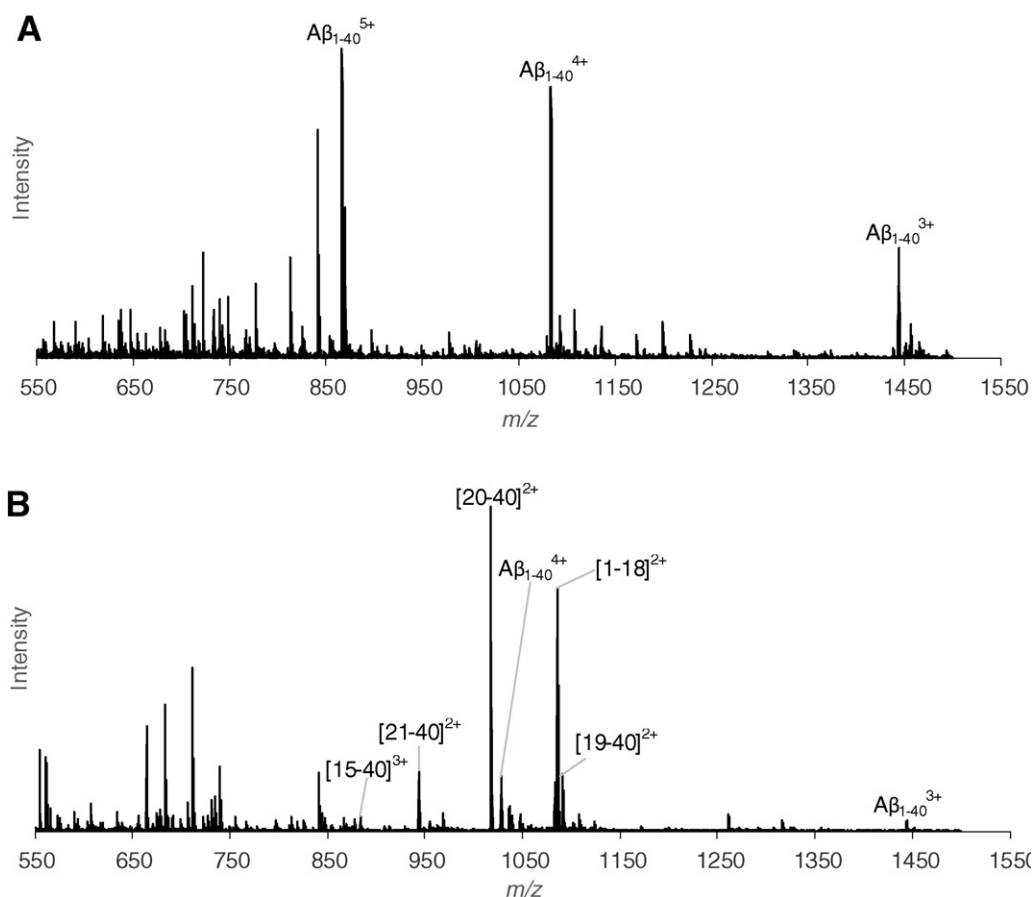

Fig. 6. Aβ fragments aggregate in time and are detected in the pellet of the Aβ$_{1-40}$-IDE sample. IDE (36 nM) was added to aggregated Aβ$_{1-40}$ (10 μM), that was pre-incubated for 24 h at 37 °C, and ESI-MS spectra of the pellet fractions (obtained after 15 min of centrifugation at 13,200 rpm) were obtained after (A) 1 h and (B) 24 h of incubation with IDE. Whereas the pellet fraction only displayed ion peaks corresponding to full-length Aβ$_{1-40}$ after 1 h of IDE incubation, cleavage fragments were observed in the pellet after 48 h of incubation, indicating that generated Aβ fragments aggregate in time.
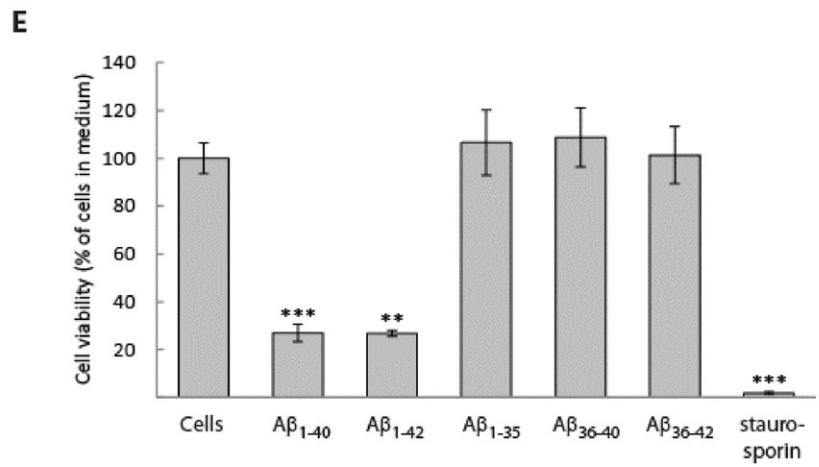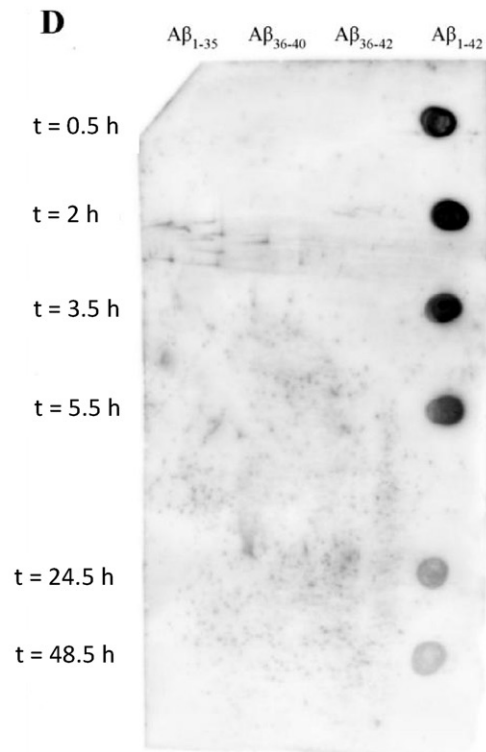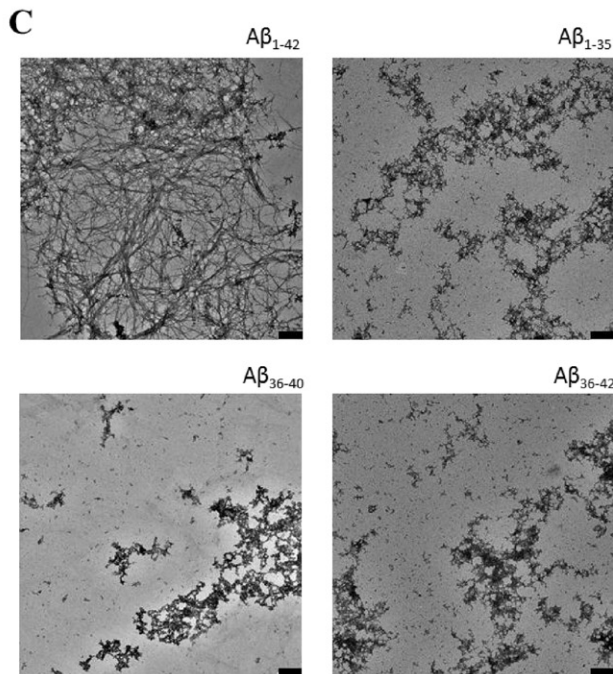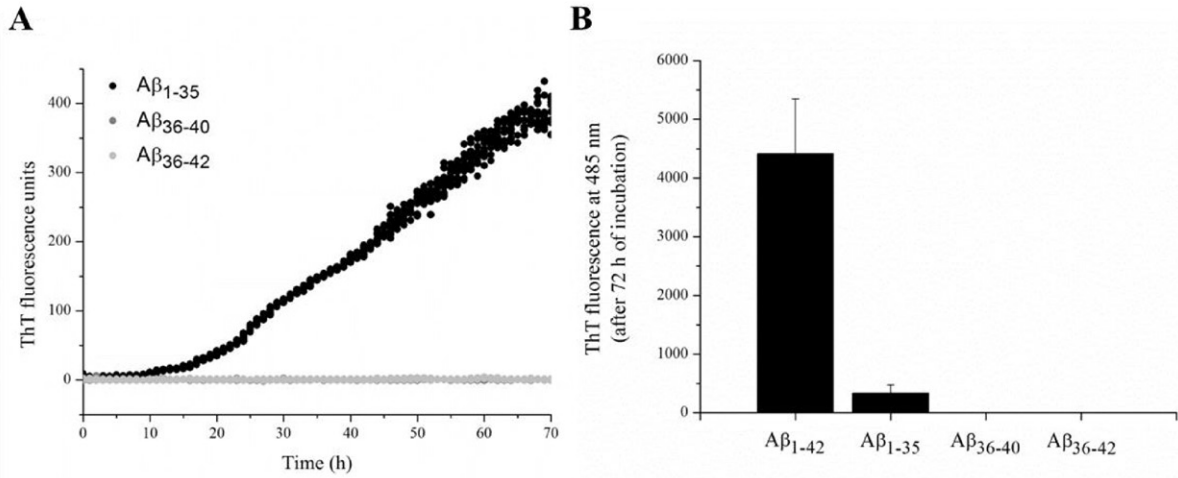
Author contributions

EH, FC, NvN, and KB designed and performed research, analysed data, and wrote the paper. JR performed research and analysed data.

Transparency Document

The Transparency document associated with this article can be found, in online version.

Appendix A. Supplementary data

Supplementary data to this article can be found online at http://dx.doi.org/10.1016/j.bbagen.2016.03.010.

References

[1] K.G. Mawuenyega, W. Sigurdson, V. Ovod, L. Munsell, T. Kasten, J.C. Morris, K.E. Yarasheski, R.J. Bateman, Decreased clearance of CNS beta-amyloid in Alzheimer's disease, Science 330 (2010) 1774.

[2] K.R. Wildsmith, M. Holley, J.C. Savage, R. Skerrett, G.E. Landreth, Evidence for impaired amyloid β clearance in Alzheimer's disease, Alzheimers Res. Ther. 5 (2013) 33.

[3] J.S. Jacobsen, T.A. Comery, R.L. Martone, H. Elokdah, D.L. Crandall, A. Oganesian, S. Aschmies, Y. Kirksey, C. Gonzales, J. Xu, H. Zhou, K. Atchison, E. Wagner, M.M. Zaleska, I. Das, R.L. Arias, J. Bard, D. Riddell, S.J. Gardell, M. Abou-Gharbia, A. Robichaud, R. Magolda, G.P. Vlasuk, T. Bjornsson, P.H. Reinhart, M.N. Pangalos, Enhanced clearance of Abeta in brain by sustaining the plasmin proteolysis cascade, Proc. Natl. Acad. Sci. U. S. A. 105 (2008) 8754–8759.

[4] C.I. Webster, M. Burrell, L.L. Olsson, S.B. Fowler, S. Digby, A. Sandercock, A. Snijder, J. Tebbe, U. Haupts, J. Grudzinska, L. Jermutus, C. Andersson, Engineering neprilysin activity and specificity to create a novel therapeutic for Alzheimer's disease, PLoS One 9 (2014), e104001.

[5] S. Howell, J. Nalbantoglu, P. Crine, Neutral endopeptidase can hydrolyze beta-amyloid(1-40) but shows no effect on beta-amyloid precursor protein metabolism, Peptides 16 (1995) 647–652.

[6] I.V. Kurochkin, S. Goto, Alzheimer's beta-amyloid peptide specifically interacts with and is degraded by insulin degrading enzyme, FEBS Lett. 345 (1994) 33–37.

[7] J.R. McDermott, A.M. Gibson, Degradation of Alzheimer's beta-amyloid protein by human and rat brain peptidases: involvement of insulin-degrading enzyme, Neurochem. Res. 22 (1997) 49–56.

[8] N. Iwata, S. Tsubuki, Y. Takaki, et al., Identification of the major Abeta1-42-degrading catabolic pathway in brain parenchyma: suppression leads to biochemical and pathological deposition, Nat. Med. 6 (2000) 143–150.

[9] N. Iwata, S. Tsubuki, Y. Takaki, et al., Metabolic regulation of brain Aβ by neprilysin, Science 2929 (2001) 1550–1552.

[10] L. Bertram, D. Blacker, K. Mullin, et al., Evidence for genetic linkage of Alzheimer's disease to chromosome 10q, Science 290 (2000) 2302–2303.

[11] S. Fukami, K. Watanabe, N. Iwata, et al., Abeta-degrading endopeptidase, neprilysin, in mouse brain: synaptic and axonal localization inversely correlating with Abeta pathology, Neurosci. Res. 43 (2002) 39–56.

[12] D.G. Cook, J.B. Leverenz, P.J. McMillan, et al., Reduced hippocampal insulin-degrading enzyme in late-onset Alzheimer's disease is associated with the apolipoprotein E-epsilon4-allele, Am. J. Pathol. 162 (2003) 313–319.

[13] E.S. Song, L.B. Hersh, Insulysin: an allosteric enzyme as a target for Alzheimer's disease, J. Mol. Neurosci. 25 (2005) 201–206.

[14] A. Caccamo, S. Oddo, M.C. Sugarman, Y. Akbari, F.M. LaFerla, Age- and region dependent alterations in Abeta-degrading enzymes: implications for Abeta-induced disorders, Neurobiol. Aging 26 (2005) 645–654.

[15] R. Madani, R. Poirier, D.P. Wolfer, et al., Lack of neprilysin suffices to generate murine amyloid-like deposits in the brain and behavioral deficit in vivo, J. Neurosci. Res. 84 (2006) 1871–1878.

[16] F. Authier, B.I. Posner, J.J. Bergeron, Insulin-degrading enzyme, Clin. Invest. Med. 19 (1996) 149–160.

[17] W.C. Duckworth, R.G. Bennett, F.G. Hamel, Insulin degradation: progress and potential, Endocr. Rev. 19 (1998) 608–624.

[18] R. Parthasarathy, K.M. Chow, Z. Derafshi, et al., Reduction of amyloid-beta levels in mouse eye tissues by intra-vitreally delivered neprilysin, Exp. Eye Res. 138 (2015) 134–144.

[19] K. Vekrellis, Z. Ye, W.Q. Qiu, et al., Neurons regulate extracellular levels of amyloid beta-protein via proteolysis by insulin-degrading enzyme, J. Neurosci. 20 (2000) 1657–1665.

[20] S.S. Kukday, S.P. Manandhar, M.C. Ludley, M.E. Burriss, B.J. Alper, W.K. Schmidt, Cell-permeable, small-molecule activators of the insulin-degrading enzyme, J. Biomol. Screen. 17 (2012) 1348–1361.

[21] C. Cabrol, M.A. Huzarska, C. Dinolfo, M.C. Rodriguez, L. Reinstatler, J. Ni, L.-A. Yeh, G.D. Cuny, R.L. Stein, D.J. Selkoe, Small-molecule activators of insulin-degrading enzyme discovered through high-throughput compound screening, PLoS One 4 (2009), e5274.

[22] B. Çakir, O. Dağliyan, E. Dağyildiz, İ. Bariş, I.H. Kavakli, S. Kizilel, M. Türkay, Structure based discovery of small molecules to regulate the activity of human insulin degrading enzyme, PLoS One 7 (2012), e31787.

[23] K. Numata, D.L. Kaplan, Mechanisms of enzymatic degradation of amyloid beta microfibrils generating nanofilaments and nanospheres related to toxicity, Biochemistry 49 (2010) 3254–3260.

[24] V. Chesneau, K. Vekrellis, M.R. Rosner, D.J. Selkoe, Purified recombinant insulin-degrading enzyme degrades amyloid beta-protein but does not promote its oligomerization, Biochem. J. 351 (Pt 2) (2000) 509–516.

[25] L. Morelli, R. Llovera, S.A. Gonzalez, J.L. Affranchino, F. Prelli, B. Frangione, J. Ghiso, E.M. Castano, Differential degradation of amyloid beta genetic variants associated with hereditary dementia or stroke by insulin-degrading enzyme, J. Biol. Chem. 278 (2003) 23221–23226.

[26] A. Mukherjee, E. Song, M. Kihiko-Ehmann, J.P. Goodman, J.S. Pyrek, S. Estus, L.B. Hersh, Insulysin hydrolyzes amyloid beta peptides to products that are neither neurotoxic nor deposit on amyloid plaques, J. Neurosci. 20 (2000) 8745–8749.

[27] C. Haass, D.J. Selkoe, Soluble protein oligomers in neurodegeneration: lessons from the Alzheimer's amyloid beta-peptide, Nat. Rev. Mol. Cell Biol. 8 (2007) 101–112.

[28] K. Broersen, W. Jonckheere, J. Rozenski, A. Vandersteen, K. Pauwels, A. Pastore, F. Rousseau, J. Schymkowitz, A standardized and biocompatible preparation of aggregate-free amyloid beta peptide for biophysical and biological studies of Alzheimer's disease, Protein Eng. Des. Sel. 24 (2011) 743–750.

[29] G. Grasso, The use of mass spectrometry to study amyloid-β peptides, Mass Spectrom. Rev. 30 (2011) 347–365.

[30] F. Delaglio, S. Grzesiek, G.W. Vuister, G. Zhu, J. Pfeifer, A. Bax, NMRPipe: a multidimensional spectral processing system based on UNIX pipes, J. Biomol. NMR 6 (1995) 277–293.

[31] W.F. Vranken, W. Boucher, T.J. Stevens, R.H. Fogh, A. Pajon, M. Llinas, E.L. Ulrich, J.L. Markley, J. Ionides, E.D. Laue, The CCPN data model for NMR spectroscopy: development of a software pipeline, Proteins 59 (2005) 687–696.

[32] A.-M. Fernandez-Escamilla, F. Rousseau, J. Schymkowitz, L. Serrano, Prediction of sequence-dependent and mutational effects on the aggregation of peptides and proteins, Nat. Biotechnol. 22 (2004) 1302–1306.

[33] R. Kayed, E. Head, J.L. Thompson, T.M. McIntire, S.C. Milton, C.W. Cotman, C.G. Glabe, Common structure of soluble amyloid oligomers implies common mechanism of pathogenesis, Science 300 (2003) 486–489.

[34] M. Biancalana, S. Koide, Molecular mechanism of thioflavin-T binding to amyloid fibrils, Biochim. Biophys. Acta 1804 (2010) 1405–1412.

[35] Y. Shen, A. Joachimiak, M.R. Rosner, W.J. Tang, Structures of human insulin-degrading enzyme reveal a new substrate recognition mechanism, Nature 443 (2006) 870–874.

[36] L.A. McCord, W.G. Liang, E. Dowdell, V. Kalas, R.J. Hoey, A. Koide, S. Koide, W.J. Tang, Conformational states and recognition of amyloidogenic peptides of human insulin-degrading enzyme, Proc. Natl. Acad. Sci. U. S. A. 110 (2013) 13827–13832.

[37] E. Malito, L.A. Ralat, M. Manolopoulou, J.L. Tsay, N.L. Wadlington, W.J. Tang, Molecular bases for the recognition of short peptide substrates and cysteine-directed modifications of human insulin-degrading enzyme, Biochemistry 47 (2008) 12822–12834.

[38] E. Malito, R.E. Hulse, W.J. Tang, Amyloid beta-degrading cryptidases: insulin degrading enzyme, presequence peptidase, and neprilysin, Cell. Mol. Life Sci. 65 (2008) 2574–2585.

Fig. 7. IDE-induced Aβ peptide fragments form amorphous aggregates with less/no staining for ThT. (A) Aggregation propensity of peptides monitored by ThT fluorescence, at 37 °C. The aggregation of Aβ$_{1-35}$ is shown by a sigmoidal ThT fluorescence curve and a lag phase of approximately 10 h. In contrast, shorter peptides Aβ$_{36-40}$ and Aβ$_{36-42}$ do not form ThT-positive aggregates. (B) ThT intensities after 72 h of incubation. (C) After 24 h incubation time at a concentration of 10 μM, TEM images depict a dense fibril network for Aβ$_{1-42}$, whereas the peptide fragments form smaller aggregates with an amorphous-like appearance. Scale bars represent 500 nm. (D) Dotblot analysis shows A11 intensity for Aβ$_{1-42}$, in particular for the early aggregation species (t = 0–5 h). No A11 intensity was detected for any of the peptide fragments. (E) Aggregated IDE-generated Aβ fragments Aβ$_{1-35}$, Aβ$_{36-40}$ and Aβ$_{36-42}$ are not cytotoxic upon incubation at a concentration of 25 μM with neuroblastoma SH-SY5Y cells. Controls include a 2 μM solution of staurosporine, full-length Aβ$_{1-40}$ and Aβ$_{1-42}$ and cells incubated with buffer.

[39] M. Zeeb, J. Balbach, Protein folding studied by real-time NMR spectroscopy, Methods 34 (2004) 65–74.

[40] N.L. Fawzi, J. Ying, D.A. Torchia, G.M. Clore, Kinetics of amyloid beta monomer-to-oligomer exchange by NMR relaxation, J. Am. Chem. Soc. 132 (2010) 9948–9951.

[41] N.L. Fawzi, J. Ying, R. Ghirlando, D.A. Torchia, G.M. Clore, Atomic-resolution dynamics on the surface of amyloid-β protofibrils probed by solution NMR, Nature 480 (2011) 268–272.

[42] L. Sánchez, S. Madurga, T. Pukala, M. Vilaseca, C. López-Iglesias, C.V. Robinson, E. Giralt, N. Carulla, Aβ40 and Aβ42 amyloid fibrils exhibit distinct molecular recycling properties, J. Am. Chem. Soc. 133 (2011) 6505–6508.

[43] G. Grasso, P. Mineo, E. Rizzarelli, G. Spoto, MALDI, AP/MALDI and ESI techniques for the MS detection of amyloid β-peptides, Int. J. Mass Spectrom. 282 (2009) 50–55.

[44] J. Pannee, U. Törnqvist, A. Westerlund, M. Ingelsson, L. Lannfelt, G. Brinkmalm, R. Persson, J. Gobom, J. Svensson, P. Johansson, H. Zetterberg, K. Blennow, E. Portelius, The amyloid-β degradation pattern in plasma—a possible tool for clinical trials in Alzheimer's disease, Neurosci. Lett. 573 (2014) 7–12.

[45] N. Kaneko, R. Yamamoto, T.A. Sato, K. Tanaka, Identification and quantification of amyloid beta-related peptides in human plasma using matrix-assisted laser desorption/ionization time-of-flight mass spectrometry, Proc. Jpn. Acad. Ser. B Phys. Biol. Sci. 90 (2014) 104–117.

[46] E. Portelius, A. Westman-Brinkmalm, H. Zetterberg, K. Blennow, Determination of beta-amyloid peptide signatures in cerebrospinal fluid using immunoprecipitation-mass spectrometry, J. Proteome Res. 5 (2006) 1010–1016.

[47] E. Portelius, N. Bogdanovic, M.K. Gustavsson, I. Volkmann, G. Brinkmalm, H. Zetterberg, B. Winblad, K. Blennow, Mass spectrometric characterization of brain amyloid beta isoform signatures in familial and sporadic Alzheimer's disease, Acta Neuropathol. 120 (2010) 185–193.

[48] J.P. Maianti, A. McFedries, Z.H. Foda, R.E. Kleiner, X.Q. Du, M.A. Leissring, W.J. Tang, M.J. Charron, M.A. Seeliger, A. Saghatelian, D.R. Liu, Anti-diabetic activity of insulin-degrading enzyme inhibitors mediated by multiple hormones, Nature 511 (2014) 94–98.

[49] A.A. Reinke, J.E. Gestwicki, Insight into amyloid structure using chemical probes, Chem. Biol. Drug Des. 77 (2011) 399–411.

[50] L. Hou, H. Shao, Y. Zhang, H. Li, N.K. Menon, E.B. Neuhaus, J.M. Brewer, I.J. Byeon, D.G. Ray, M.P. Vitek, T. Iwashita, R.A. Makula, A.B. Przybyla, M.G. Zagorski, Solution NMR studies of the A beta(1-40) and A beta(1-42) peptides establish that the Met35 oxidation state affects the mechanism of amyloid formation, J. Am. Chem. Soc. 126 (2004) 1992–2005.

[51] H.A. Scheidt, I. Morgado, S. Rothemund, D. Huster, M. Fändrich, Solid-state NMR spectroscopic investigation of Aβ protofibrils: implication of a β-sheet remodeling upon maturation into terminal amyloid fibrils, Angew. Chem. Int. Ed. Engl. 50 (2011) 2837–2840.